An application of wavelet analysis to paleoproductivity records from the Southern Ocean

Asok K. Sen [a,*], Gabriel M. Filippelli [b], José-Abel Flores [c]

[a] Department of Mathematical Sciences, Indiana University Purdue University, 402 N. Blackford Street, Indianapolis, IN 46202, USA
[b] Department of Earth Sciences, Indiana University Purdue University, 723 West Michigan Street, Indianapolis, IN 46202, USA
[c] Department of Geology, Faculty of Sciences, University of Salamanca, Salamanca 37008, Spain

ARTICLE INFO

ABSTRACT

We have performed wavelet analysis of the paleoproductivity records from the southeastern Atlantic sector of the Southern Ocean. In particular, we have applied a continuous wavelet transform to the phosphorus-to-titanium (P/Ti) ratios obtained from the Ocean Drilling Program (ODP) Sites 1089 and 1094 over the past ~600 kyr, and computed their wavelet power spectra in order to elucidate the spectral–temporal aspects of phosphorus deposition at these sites. Because data are unevenly sampled in time, they are first resampled using a uniform sampling interval prior to wavelet analysis. The wavelet power spectra of the P/Ti data are presented on a time-period plane from which the dominant periodicities of P export and their duration in time are discerned by visual inspection. Our results indicate that at the ODP Site 1089, the strongest P export occurs within a periodic band with the most dominant period of ~100 kyr, which corresponds to the eccentricity period of Milankovitch cyclicity. On the other hand, at the ODP Site 1094, which is completely covered with ice during the glacial times, the strongest periodicity of P export is found to be around 82 kyr. This periodicity is twice the period of the 41-kyr Milankovitch obliquity cycle, implying that obliquity forcing drives the productivity at this site in a period doubling scenario. Given the strong influence of ice cover at this site, another implication is that sea ice extent itself is strongly influenced by the obliquity signal, and productivity simply responds to the availability of ice-free conditions. We have also performed wavelet analysis of the carbonate production data at the ODP Site 1089, and found a dominant periodicity of ~100 kyr. In addition, a few weaker decadal-scale periodicities are observed in both P/Ti and carbonate data which can be linked to Milankovitch cycles.

© 2009 Elsevier Ltd. All rights reserved.

1. Introduction

A characteristic feature of paleoceanographic records derived from marine sediment cores is their uneven data sampling in time. Uneven data sampling is encountered in many other applications (Carbonell et al., 1992; Van Dongen et al., 1999). For example, in astronomical records, data are often unevenly sampled due to gaps in observations caused by external factors such as weather conditions, telescope malfunction, etc.

To perform spectral analysis of unevenly sampled data, the traditional Fourier transform has been extended by Lomb (1976) and Scargle (1989). Their extension is commonly referred to as the Lomb–Scargle periodogram (LSP) technique. It was originally applied to astronomical records but has been used later in other situations (Van Dongen et al., 1999), including paleoclimatic time series analysis (Schulz and Stattegger, 1997). It should be noted that, since Fourier transform is a purely frequency domain approach, the LSP technique can determine only the periodicities in the data but not the time intervals over which such periodicities may persist.

An alternate approach to treat unevenly sampled data is to resample the data with a uniform sampling interval. A simple way to do this is to use linear interpolation. De Waele and Broersen (2000) have shown that linear interpolation is a robust resampling method although it provides a signal whose standard deviation is biased with a systematic error. Recently, Thiebaut and Roques (2005) have demonstrated that this error can be corrected by using the nearest neighbor resampling. It should be pointed out, however, that depending on the signal characteristics, interpolating the data may lead to aliasing, with underestimation of the high frequencies.

After an unevenly spaced signal is resampled with a uniform sampling interval, the traditional Fourier transform can be used to determine its periodicities. However, as indicated above, a Fourier transform cannot reveal the temporal variations of

* Corresponding author. Tel.: +1 317 274 6922; fax: +1 317 274 3460.
  E-mail addresses: asen@iupui.edu (A.K. Sen), gfilippe@iupui.edu
(G.M. Filippelli), flores@usal.es (J.A. Flores).

these periodicities. This limitation may be overcome by using a windowed or a short-time Fourier transform (STFT), i.e., by windowing a small segment of the signal at a time and then sliding the window in time. It is important to note that STFT uses a fixed-size window, and thus suffers from the following drawback: for a given signal, the frequency resolution may be low or the time resolution may be poor, depending on the choice of the window size (Addison, 2002). An efficient way to delineate the temporal variations of periodicities is to use wavelet analysis. Recently, Thiebaut and Roques (2005) used a wavelet-based approach for time–frequency analysis of astronomical time series after interpolating the data using the nearest neighbor resampling.

The purpose of this paper is to perform a wavelet analysis of the phosphorus-to-titanium (P/Ti) ratio data from two sites (ODP Sites 1089 and 1094) in the southeastern Atlantic sector of the Southern Ocean. Our goal is to elucidate the influence of climatic cycles on paleoproductivity in the Southern Ocean. We apply a continuous wavelet transform (CWT) to the P/Ti time series and compute the wavelet power spectra (WPS) in order to describe the spectral–temporal aspects of excess P delivery to these sites. From the WPS of P/Ti data, the dominant periodicities of excess P and their duration in time can be readily discerned by visual inspection. We also examine sedimentary carbonate production at the ODP Site 1089 using wavelet analysis. For comparison, the power spectra of the various time series calculated with a Fourier transform are also presented here.

2. Study site and data acquisition

The Southern Ocean is delimited northward by the mean latitude of the Subtropical Convergence Zone (~45°S). The ODP Site 1089 (4620 m water depth, 41°S, 10°E) was recovered during Ocean Drilling Program Leg 177, and is located within the Subantarctic Zone, south of the subtropical front (Gersonde et al., 1999). The drilling site itself is located in the southern Cape Basin. Pleistocene sediments at this site are dominated by interbedded carbonate and opal oozes, and exhibit a Pacific Pleistocene sedimentation pattern with glacial intervals marked by high carbonate content (Hodell et al., 2001). The ODP Site 1094 (2807 m water depth, 53°S, 5°E) is located south of the polar front, and is further south of the ODP Site 1089 (Gersonde et al., 1999). This site was completely covered with sea ice during full glacial times (Gersonde and Zielinski, 2000). The locations of these sites relative to the ocean floor topography are shown on a site map in Fig. 1.

In order to assess phosphorus accumulation at the ODP Sites 1089 and 1094, we analyzed the P/Ti ratio at these sites. The P/Ti ratio reflects excess P delivery to the seafloor not supported by terrigenous components. Therefore, an increase in P/Ti ratio implies higher phosphorus sedimentation to the seafloor from biological processes. Even though the P/Ti ratio does not directly correlate with the phosphorus mass balance, it limits the effect of sediment focusing on biasing accumulation rate records in drift settings (Latimer and Filippelli, 2001), yet reflects biological export production. We have also analyzed the carbonate data at Southern Ocean Site 1089 and used it an as independent proxy at this site.

Geochemical analysis of the samples collected at different depths at the above two sites was carried out as follows. After completely digesting the samples using a CEM Corporation MDS 2000 microwave digestion system, they were analyzed by inductively coupled plasma-atomic emission spectroscopy (ICP-AES). A Leeman Labs P950 ICP-AES was used with a CETAC Corporation AT5000+ ultrasonic nebulizer to determine the total elemental concentrations. Ten percent of the samples were
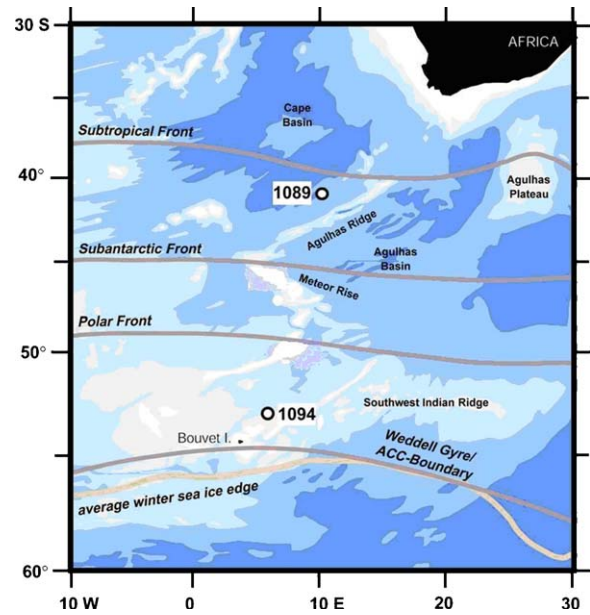

Fig. 1. Location map of ODP Sites 1089 and 1094 in the Southern Ocean.

analyzed as randomly chosen replicates, which agreed within 7% for all the elements analyzed. The phosphorus concentrations were normalized with respect to the titanium concentrations (see Filippelli et al., 2007 for details). Ages were assigned for samples by calculating linear sedimentation rates between age control points based on oxygen isotope stratigraphy (Hodell et al., 2001). As indicated above, the paleoproductivity records involve uneven data sampling. For the wavelet analysis presented here, we first resample the time series uniformly with 1-kyr sampling interval using a linear interpolation scheme with the nearest neighbor sampling.

3. Wavelet analysis

We have performed wavelet analysis of the time series of P/Ti ratios at the ODP Sites 1089 and 1094, and of carbonate data at the ODP Site 1089. Carbonate data at the site 1094 is of insufficient resolution to perform a meaningful spectral analysis. Wavelets have been used for signal analysis in a wide variety of applications including geology and geophysics (Gencay et al., 2001; Grinsted et al., 2004; Kumar and Foufoula-Georgiou, 1997; McAteer et al., 2004; Percival and Walden, 2001; Prokoph and Barthelmes, 1996; Prokoph et al., 2000; Torrence and Compo, 1998). Wavelet analysis maps a time series into a time–frequency plane, and enables identification of both the dominant modes of variability and how those modes vary with time.

Our analysis is based on a continuous wavelet transform. Using a variable-size window in a time–frequency plane, CWT provides an efficient approach by which both time and frequency resolutions can be adjusted in an adaptive fashion. A wavelet transform uses a window that narrows when focusing on small-scale or high-frequency features of the signal and widens on large-scale or low-frequency features, analogous to a zoom lens (Kumar and Foufoula-Georgiou, 1997). In our recent work, we have used CWT to study (i) local field potentials recorded from patients with Parkinson's disease (Sen and Dostrovsky, 2007), and (ii) seizure EEG in kindled epileptic rats (Sen et al., 2007), (iii) cycle-to-cycle pressure variations in spark ignition and diesel engines (Sen et al., 2008a, b), (iv) riverflow variability in England and Wales (Sen, 2009), and (v) periodicities in Late Holocene stalagmite records

from Ortigosa caves in Spain (Muñoz et al., 2009). An important advantage of wavelet analysis is that in addition to detecting the inherent periodicities in the data, it can delineate the time intervals over which the various periodicities persist.

We briefly describe the method of wavelet analysis of a time series using CWT and then apply it to the paleoproductivity time series recorded from the ODP Sites 1089 and 1094. A wavelet is a small wave with zero mean and finite energy. The continuous wavelet transform of a time series with respect to a wavelet $\psi(\tau)$ is defined as its convolution with $\psi(\tau)$. The wavelet $\psi(\tau)$ is referred to as an analyzing wavelet or a mother wavelet. The convolution involves a scaled and translated version of $\psi(\tau)$. The scale parameter controls dilation or contraction of the wavelet, and the translation parameter specifies the location of the wavelet in time. The amount of signal energy contained at a specific scale and location is given by the square of the modulus of the CWT. This energy density function is called the wavelet power spectrum (WPS) of the time series. The WPS which depends on both scale and time is represented by a surface. By taking contours of this surface and plotting them on a plane, a time-scale representation of the wavelet power spectrum may be derived. From a time-scale representation, the various periodicities can be identified by visual inspection. In our analysis, we used a complex Morlet wavelet as the mother wavelet. A Morlet wavelet consists of a plane wave modulated by a Gaussian function and is described by: $\psi(\tau) = \pi^{-1/4} e^{i\omega_0 \tau} e^{-\tau^2/2}$. The parameter ω_0 is the center frequency, also referred to as the order of the wavelet. The value of ω_0 controls the number of oscillations that is present in the mother wavelet, and thus influences the frequency and time resolution of the corresponding wavelet transform. A larger value of ω_0 provides a higher frequency resolution, whereas a smaller value improves the time resolution. In our analysis, we have used a Morlet wavelet with $\omega_0 = 6$. This value of ω_0 offers a good balance between time and frequency localizations. For $\omega_0 = 6$, the Fourier period is approximately equal to the scale s. In other words, with this choice of ω_0 the terms scale and period may be used interchangeably for interpretation of the results.

4. Results and discussion

First we consider the P/Ti record at the ODP Site 1089. The time series of this data is depicted in Fig. 2(a) for a time interval of 583 kyr. Fig. 2(b) shows the wavelet power spectrum of this time series on a time-period plane. For comparison, the time series has been overlaid on the WPS. The periodicities in the time series and their duration can be readily discerned from the WPS. In this figure, the thick contour lines enclose regions of greater than 95% confidence for a red-noise process, and the thin U-shaped curve defines the cone of influence (COI). The cross-hatched region below the U-shaped curve is referred to as the COI. Because the time series we are dealing with is finite, the wavelet transform suffers from edge effects at its two ends resulting in a COI in the wavelet power spectrum. At a given period, the extent of the COI from each end of the time series is defined as the e-folding time of the autocorrelation of wavelet power (Torrence and Compo, 1998). Within the COI, the wavelet power for a discontinuity at the edges is reduced by a factor of e^{-2}. As a consequence, the wavelet power spectrum inside the COI is unreliable and should be interpreted with caution. This is a practical limitation of wavelet analysis. The edge effects are more pronounced at larger scales (or periods) as the influence of each wavelet extends further in time and larger parts of the discontinuities will enter the analysis (De Moortel et al., 2002). For a periodicity to be considered, it must last for at least one full oscillation outside the COI at greater than 95% confidence. It is apparent from Fig. 2(b) that the strongest
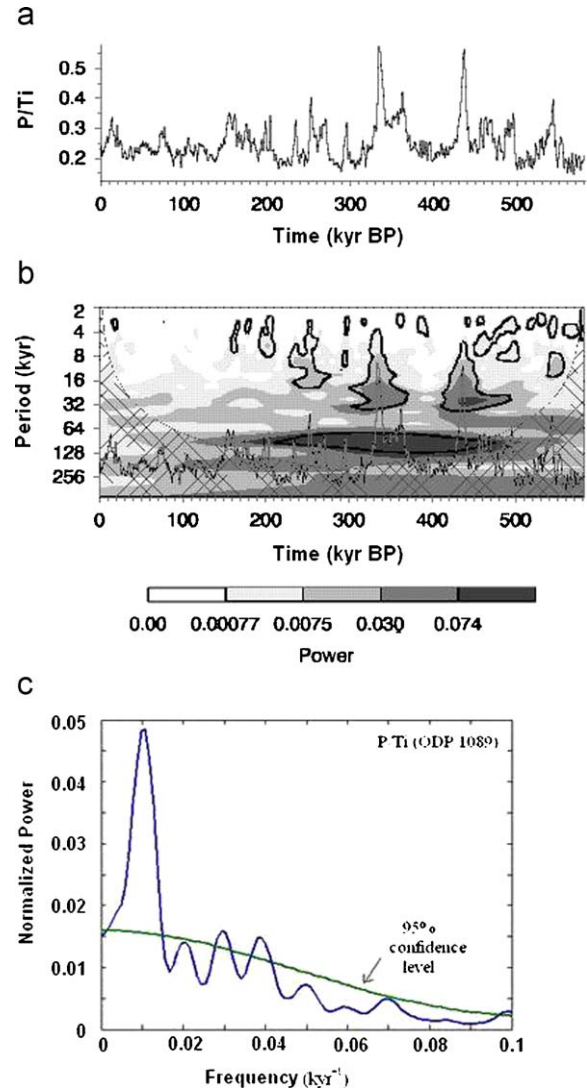

Fig. 2. (a) Time series of phosphorus-to-titanium ratios (P/Ti) at ODP Site 1089 (resampled uniformly with a 1-kyr sampling interval). (b) Wavelet power spectrum (WPS) of P/Ti data shown in (a). Thick contour lines denote 95% confidence level and the cross-hatched region below the thin U-shaped curve represents the cone of influence (COI). For comparison, the time series has been overlaid on the WPS. (c) Power spectrum of time series shown in (a). It is apparent from the WPS that the strongest periodicities are in the band between the periods of 79 and 121 kyr, with the highest power in this band around the 100-kyr period. Weaker cycles with periods of 23 and 30 kyr are also seen in this figure.

periodicities are in the band between the periods of 79 and 121 kyr, with highest power at the period of approximately 100 kyr. This dominant period corresponds to the period of Milankovitch glacial–interglacial cycle (Milankovitch, 1941; Berger, 1988; Imbrie et al., 1993). As seen from this figure, the above periodic band persists in time from approximately 220 to 460 kyr, lasting more than two full cycles. In Fig. 2(b), we also observe two weaker periodic bands on the decadal time scale, with periods around 23 and 30 kyr. The band around the 23-kyr period spans more than two cycles between 320 and 370 kyr. The 30-kyr periodic band persists approximately from 415 to 490 kyr, also spanning more than two full cycles. As mentioned in the Introduction, we have computed the power spectrum of the P/Ti time series using the Fourier transform. The power spectrum is depicted in Fig. 2(c), which reveals the various periodicities mentioned above. Note, however, that the power spectrum cannot delineate the duration of any of these periodicities.

Milankovitch's astronomical theory of long-term changes in orbital parameters predicts quasiperiodic variations of eccentricity, obliquity, and precession of the equinoxes with dominant frequencies centered around 100, 41 and 23 kyr, respectively. The 23-kyr period observed in the P/Ti data correspond to the precessional frequency of the Milankovitch cycle, whereas the 30-kyr period may arise from the interaction of multiple forcing with different orbital frequencies producing heterodynes, as the combination of the glacial–interglacial frequency of $0.01 \, kyr^{-1}$ and precession frequency of $0.043 \, kyr^{-1}$ results in a new frequency equal to the difference between the two $(0.033 \, kyr^{-1})$ (Holbourn et al., 2005). In general, the spectral characteristics of the P/Ti data at the ODP Site 1089 are similar to the observations based on the oxygen record from this site (e.g., Hodell et al., 2001), supporting the strong link between paleoproductivity and variations in oceanic nutrient mass balances noted by Filippelli et al. (2007).

Next, we consider the P/Ti record at the ODP Site 1094 for which the time series is shown in Fig. 3(a). Recall that this site was completely covered with ice during the glacial times. The WPS of the time series is illustrated in Fig. 3(b) in which the times series has been overlaid for comparison. This figure reveals that the most dominant periodicities at this site lie in the band between the periods of 68 and 96 kyr, with the highest power at the period of 82 kyr. This periodic band exists from approximately 130–395 kyr in time. In addition, decadal-scale periodicities around 23-, 30- and 41-kyr periods are seen in this figure. The 41-kyr period corresponds to the Milankovitch obliquity cycle, whereas the 23- and 30-kyr periods are, respectively, consequences of the Milankovitch precessional cycle and the heterodyning effect alluded to above. All the cycles are also observed in the power spectrum of the time series displayed in Fig. 3(c). The time intervals over which these oscillations persist are as follows: 23-kyr period from 310 to 350 kyr, 30-kyr period between 210 and 260 kyr, and 41-kyr period from 180 to 350 kyr, with each of the periodicities spanning two or more cycles. An interesting aspect of the spectral characteristics from this site is the presence of the 82-kyr cycle, whose period is twice the period of the 41-kyr obliquity signal. This would imply that obliquity forcing drives paleoproductivity at this site in a period doubling scenario. Given the strong influence of ice cover at this site, another implication is that sea ice extent itself is strongly influenced by the obliquity signal, and productivity simply responds to the availability of ice-free conditions. As in the case of the P/Ti data at the ODP Site 1089, the wavelet power spectrum in this case was able to detect this dominant periodicity of 82 kyr within the region that lies outside the COI. In order to confirm that this cycle was not caused by the two large spikes in the data, we have analyzed the de-spiked data and found that the 82-kyr cycle was still present.

Finally, we consider the carbonate production record at the ODP Site 1089. Figs. 4(a) and (b) depict, respectively, the carbonate time series and its WPS. As before, the time series has been overlaid on the WPS, for comparison. Analogous to Fig. 2(b), the strongest oscillatory power is in a periodic band around the 100-kyr period, which corresponds to the eccentricity signal of Milankovitch cyclicity in the glacial–interglacial cycles. This periodic band spans over three cycles from approximately 145 to 460 kyr, outside the cone of influence. In addition, there are weaker periodicities on the decadal time-scale around the 23-, 30- and 46-kyr periods, seen in this figure. Similar periodicities are also observed in the power spectrum shown in Fig. 4(c). As mentioned earlier, the 23-kyr cycle is the influence of the Milankovitch precessional cycle, whereas the 30-kyr period is the result of the interaction between the 100- and 23-kyr cycles. Note that the 23-kyr band persists from 315 to 365 kyr in time with more than two cycles, whereas the 30-kyr periodic band is
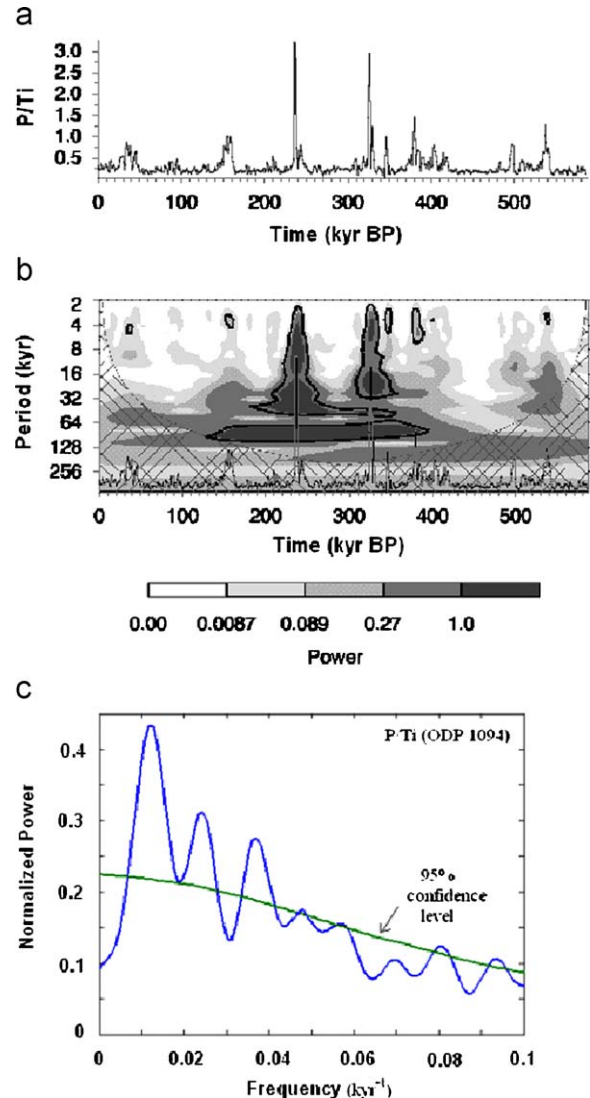

Fig. 3. (a) Time series of phosphorus-to-titanium ratios (P/Ti) at ODP Site 1094 (resampled uniformly with a 1-kyr sampling interval). (b) WPS of P/Ti data shown in (a). As in Fig. 2(b), thick contour lines denote 95% confidence level and the cross-hatched region represents the COI. For comparison, the time series has been overlaid on the WPS. (c) Power spectrum of the time series shown in (a). WPS in (b) reveals that the most dominant periodicities at this site lie in the band between the periods of 68 and 96 kyr, with the highest power in this band around the 82-kyr period. Weaker cycles with periods of 23, 30 and 41 kyr are also seen in this figure.

seen to occur between 425 and 470 kyr. The 46-kyr cycle may be the result of a period doubling phenomenon from the 23-kyr cycle. Note, however, that much of the 46-kyr period at greater than 95% confidence falls inside the COI.

In addition to a Morlet wavelet, we have used other types of mother wavelets such as the Paul and Derivative of Gausssian (DOG) wavelets (Torrence and Compo, 1998; De Moortel et al., 2004). In general, for the same order, the Morlet wavelet offers a higher frequency resolution and a lower time resolution than a Paul wavelet. Using a Paul wavelet of order 12, we have obtained WPS results that are comparable to those found with a Morlet wavelet of order 6.

4. Summary and conclusions

We have analyzed the periodicities of P/Ti ratio data obtained from the ODP Sites 1089 and 1094 in the Southern Ocean.
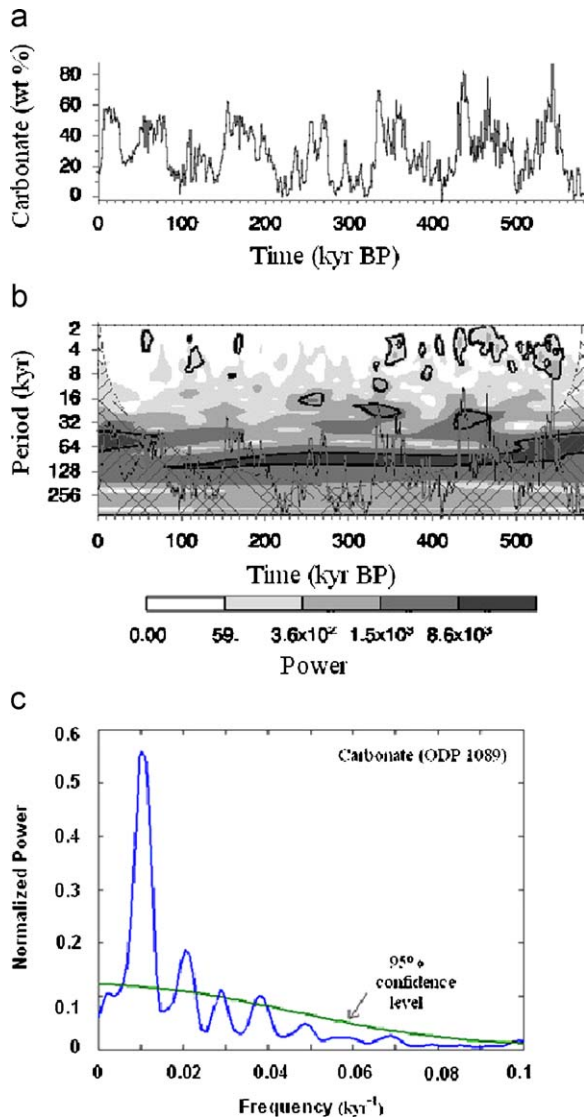
Fig. 4. (a) Time series of carbonate production at ODP Site 1089 (resampled uniformly with a 1-kyr sampling interval). (b) WPS of carbonate data shown in (a). As in Fig. 2(b), thick contour lines denote 95% confidence level and the cross-hatched region represents the COI. For comparison, the time series has been overlaid on WPS. (c) Power spectrum of the time series shown in (a). Strongest periodicities in WPS are seen in the band between the periods of 83 and 115kyr, with the highest power around the 100-kyr period. Weaker cycles with periods of 23 and 30kyr are also seen in this figure.

In addition, we have examined carbonate data from the ODP Site 1089. The data consist of unevenly sampled time series. Using linear interpolation with the nearest neighbor sampling, we resampled the data at a uniform rate of 1-kyr. Subsequently, we applied a continuous wavelet transform on the resampled data and computed their wavelet power spectra. At the ODP Site 1089, the wavelet power spectrum revealed the influence of the100-kyr Milankovitch cycle in both P/Ti and carbonate data. On the other hand, at the ODP Site 1094, which is ice-covered during glacial times, the dominant periodicity was found around the 82-kyr cycle. This periodicity may be driven by the 41-kyr obliquity cycle through a period doubling scenario. In addition, the wavelet power spectra revealed a few weaker cycles with shorter periods that are linked to Milankovitch forcing. The wavelet analysis also delineated the time intervals over which the various periodicities may persist.

References

Addison, P.S., 2002. The Illustrated Wavelet Transform Handbook. Institute of Physics Publishing, Philadelphia, 353pp.

Berger, A., 1988. Milankovitch theory and climate. Reviews in Geophysics 26, 624–657.

Carbonell, M., Oliver, R., Ballester, J.L., 1992. Power spectra of gapped time series: a comparison of several methods. Astronomy & Astrophysics 264, 350–360.

De Waele, S., Broersen, P.M.T., 2000. Error measures for resampled irregular data. IEEE Transactions on Instrumentation and Measurement 49, 216–222.

De Moortel, I., Munday, S.A., Hood, A.W., 2004. Wavelet analysis: the effect of varying basic wavelet parameters. Solar Physics 222, 203–224.

De Moortel, I., Hood, A.W., Ireland, J., 2002. Coronal seismology through wavelet analysis. Astronomy & Astrophysics 381, 311–323.

Filippelli, G.M., Latimer, J.C., Murray, R.W., Flores, J.A., 2007. Productivity records from the southern ocean and the equatorial Pacific Ocean: testing the glacial shelf-nutrient hypothesis. Deep-Sea Research Part II 54, 2443–2452.

Gencay, R., Selcuk, F., Whitcher, B., 2001. An Introduction to Wavelets and Other Filtering Methods in Finance and Economics. Academic Press, New York, 359pp.

Gersonde, R., Zielinksi, U., 2000. The reconstruction of late quaternary antarctic sea-ice distribution; the use of diatoms as a proxy for sea-ice. Paleogeography, Palaeoclimatology, Palaeoecology 162, 263–286.

Gersonde, R., Hodell, D.A., Blum, P., 1999. In: Proceedings of the Ocean Drilling Program, Initial reports, vol. 177 [CD-ROM]: College Station, TX, Ocean Drilling Program.

Grinsted, A., Moore, J.C., Jevrejeva, S., 2004. Application of the cross wavelet transform and wavelet coherence to geophysical time series. Nonlinear Processes in Geophysics 11, 561–566.

Hodell, D.A., Charles, C.D., Sierro, F.J., 2001. Late Pleistocene evolution of the ocean's carbonate system. Earth and Planetary Science Letters 192, 109–124.

Holbourn, A., Kuhnt, W., Kawamura, H., Jian, Z., Grootes, P., 2005. Orbitally paced paleoproductivity variations in the Timor Sea and Indonesian throughflow variability during the past 460 kyr. Paleoceanography 20, PA3002.

Imbrie, J., Berger, A., Boyle, E.A., Clemens, S.C., Duffy, A., Howard, W.R., Kukla, G., Kutzbach, J., Martinson, D.G., McIntyre, A., Mix, A.C., Molfino, B., Morley, J.J., Peterson, L.C., Pisias, N.G., Prell, W.L., Raymo, M.E., Shackleton, N.J., Toggweiler, J.R., 1993. On the structure and origin of major glaciation cycles 2. The 1,00,000 year cycle. Paleoceanography 8, 699–735.

Kumar, P., Foufoula-Georgiou, E., 1997. Wavelet analysis for geophysical applications. Reviews in Geophysics 35, 385–412.

Latimer, J.C., Filippelli, G.M., 2001. Terrigenous input and paleoproductivity in the Southern Ocean. Paleoceanography 16, 627–643.

Lomb, N., 1976. Least-squares frequency analysis of unequally spaced data. Astrophysics and Space Science 39, 447–462.

McAteer, R.T.J., Gallagher, P.T., Bloomfield, D.D., Williams, D.R., Mathioudakis, M., Keenan, F.P., 2004. Ultraviolet oscillations in the chromosphere of the quiet sun. Astrophysical Journal 602, 436–445.

Milankovitch, M., 1941. Canon of Insolation in the Ice-Age Problem. Royal Serbian Academy, Belgrade, 484pp. (English translation by the Israel Program for Scientific Translation, published by the US Department of Commerce and the National Science Foundation.)

Muñoz, A., Sen, A.K., Sancho, C., Genty, D., 2009. Wavelet analysis of Late Holocene stalagmite records from Ortigosa caves in Northern Spain. Journal of Cave and Karst Studies, in press.

Percival, D.P., Walden, A.T., 2001. Wavelet Methods for Time Series Analysis. Cambridge University Press, Cambridge, UK, 594pp.

Prokoph, A., Barthelmes, F., 1996. Detection of nonstationarities in geological time series: wavelet transform of chaotic and cyclic sequences. Computers & Geosciences 22, 1097–1108.

Prokoph, A., Fowler, A.D., Patterson, R.T., 2000. Evidence for periodicity and nonlinearity in a high-resolution fossil record of long-term evolution. Geology 28, 867–870.

Scargle, J.D., 1989. Studies in astronomical time series analysis III. Fourier transform, autocorrelation functions, and cross correlation functions of unevenly spaced data. Astrophysical Journal 343, 874–887.

Schulz, M., Stattegger, K., 1997. SPECTRUM: spectrum analysis of unevenly spaced paleoclimatic time series. Computers & Geosciences 23, 929–945.

Sen, A.K., Dostrovsky, J.O., 2007. Evidence of intermittency in the local field potentials recorded from patients with Parkinson's disease: a wavelet-based approach. Computational and Mathematical Methods in Medicine 8, 165–171.

Sen, A.K., Kubek, M.J., Shannon, H.E., 2007. Analysis of seizure EEG in kindled epileptic rats. Computational and Mathematical Methods in Medicine 8, 225–234.

Sen, A.K., Longwiec, R., Litak, G., Gorski, K., 2008a. Cycle-to-cycle pressure oscillations in a diesel engine. Mechanical Systems and Signal Processing 22, 362–373.

Sen, A.K., Litak, G., Taccani, R., Radu, R., 2008b. Wavelet analysis of cycle-to-cycle pressure variations in an internal combustion engine. Chaos, Solitons & Fractals 38, 886–893.

Sen, A.K., 2009. Spectral-temporal characterization of riverflow variability in England and Wales for the period 1865–2002. Hydrological Processes, in press.

Thiebaut, C., Roques, S., 2005. Time-scale and time-frequency analysis of irregularly sampled astronomical time series. EURASSIP Journal on Applied Signal Processing 15, 2486–2499.

Torrence, C., Compo, G.P., 1998. A practical guide to wavelet analysis. Bulletin of the American Meteorological Society 79, 61–78.

Van Dongen, H.P.A., Olofsen, E., Van-Hartevelt, J.H., Kruyt, E.W., 1999. Searching for biological rhythms: peak detection in the periodogram of unequally spaced data. Journal of Biological Rhythms 14, 617–620.